A COMPUTATIONAL STUDY OF MULTI-BURNER ANNULAR AERO GAS TURBINE

C. Fureby & E. Fedina
Defense Security Systems Technology, The Swedish Defense Research Agency – FOI, Stockholm, Sweden

Keywords: *gas turbine combustion, large eddy simulation, combustion instabilities*

Abstract

In this study we present results from simulations of a single sector and a fully annular multi-burner aero engine combustor. The objectives are to facilitate the understanding of the flow, mixing and combustion to help improve the combustor design and the design process as well as to demonstrate that it is now feasible to perform high-fidelity re-acting flow simulations of full annular gas turbine combustors. The simulations are performed by a combustion Large Eddy Simulation (LES) model in which all flow features larger than the grid are resolved whereas the effects of the small scale flow features on the large ones are modeled. The LES method used is validated against a range of non-reacting and reacting flow configurations a few of which are reported here. The aero engine combustor of interest is here modeled both using a conventional single sector configuration and a fully annular multi-burner configuration and the Jet-A combustion chemistry is modeled by a global three-step mechanism. The single-sector and fully annular multi-burner predictions are similar but with the fully annular multi-burner configuration showing a different combustion dynamics and thus also somewhat different time-averaged profiles of the dependent variables. For the fully annular multi-burner configuration azimuthal pressure fluctuations are observed, resulting in successive reattachment and detachment of the flames in the azimuthal direction.

1. Introduction and Background

For civilian and military aeropropulsion, including turboshaft engines for helicopters and small aircrafts, turbofans for large aircraft, and afterburning turbojets and turbofans for combat aircraft there is no realistic substitute for gas turbine engines. Modern aeropropulsion gas turbine engines usually have an annular combustion system with multiple burners sharing a common fuel supply line. Constraints on such gas turbines include velocity and temperature profiles delivered to the turbine (affecting turbine life), pressure drop across the combustor (affecting e.g. thermal efficiency), the ability to withstand flame extinction, blow-out and pressure oscillations, the ability to relight at high altitudes, unsteady thermal loads and mechanical vibrations as well as emission regulations on CO, CO_2, NO, unburned hydrocarbons as well as smoke. Although the current trend in gas turbine design is towards fuel lean and premixed conditions to reduce emissions, most aeropropulsion gas turbines makes use of spray flames. The fuel spray is usually created by passing the liquid fuel through an air-blast atomizer in which the liquid fuel film is broken up into small droplets that are sprayed into the combustor together with air under swirling conditions. Neighboring spray flames in an annular configuration interact with each other, and with the acoustic pressure field in the combustion chamber, and are further influenced by the air-flow through the dilution and film cooling holes in the liner, resulting in complex flow phenomena.

Accurate observations and quantitative measurements of these processes in realistic configurations are difficult and very expensive, and are thus in short supply. Better understanding of these flows for design modifications and exploration of the fundamental physics demands high-fidelity numerical studies in realistic configurations. Specifically, good predictive capability for swirling, turbulent reacting flows in complex geometries is necessary.

To meet these challenges in a cost- and time-effective manner, improved combustor design tools are needed that can include accurate models of turbulent flow and mixing, chemical kinetics, spray physics, thermal radiation etc. Current steady-state Reynolds Averaged Navier Stokes (RANS) combustion models, e.g. [1-2], lack the quantitative accuracy needed for reliable predictions of transient phenomena such as vortex shedding, shear layer mixing, acoustics, combustion instabilities, blow-out, self-ignition and emissions. A better approach is to use combustion Large Eddy Simulation (LES), [3-5], in which the large scales of the flow are explicitly simulated and only the small (subgrid) scales are modeled, [6]. It has been previously shown that LES captures mixing better than RANS, [2], and turbulent combustion interactions even better, [5]. Moreover, the combustion dynamics, and its effect on mixing and reaction is only captured by combustion LES. Practical combustion LES has now matured, so that single sector gas turbine combustors are routinely investigated, [7-8], whereas only a few annular gas turbine combustor LES, being able to capture all acoustic modes of relevance and interactions in the combustor, have been performed, [9-10]. It is important to further develop and demonstrate combustion LES so that these high-fidelity models soon can be utilized in the design environment. Such a design tool will dramatically reduce the test costs and produce improved, low emissions combustor designs. Here we describe the use of single sector and fully annular, multi-burner, combustion LES to study the CESAR aeropropulsion gas turbine combustor system, [11]. The results of these LES predictions are here used to examine both single sector and fully annular multi-burner configurations, and to elucidate the physical processes taking place in a fully annular multi-burner configuration.

2. Mathematical and Numerical Modeling

The mathematical model used consists of the balance equations of mass, species mass fractions, momentum and energy, describing convection, diffusion and reactions, [12]. The reactive gaseous mixture is assumed to be a linear viscous fluid with Fourier heat conduction and Fickian diffusion, [1]. The viscosity is computed from Sutherland's law and the thermal conductivity and species diffusivities are computed using the viscosity and constant Prandtl and species Schmidt numbers, respectively. The mixture thermal and caloric equations of state are obtained under the assumption that each specie is a thermally perfect gas, with tabulated formation enthalpies and specific heats, respectively, [1]. The reaction rates are computed from Guldberg-Waage's law of mass action by summation over all participating reactions, with rate constants obtained from a modified Arrhenius law, [13]. The ranges of scales present in turbulent reacting flows typically covers eight orders of magnitude, [14], with the smaller scales being less energetic but important for the chemical kinetics, and here a Large Eddy Simulation (LES), [6], model is used to filter out the small scales of motion, whilst representing their effects on the resolved scales of motion by a subgrid flow model and a subgrid turbulence chemistry interaction model, [4-5]. Here, the subgrid stress tensor and flux vectors are modeled using the mixed model, [15], whereas the sub-grid turbulence chemistry interaction terms are modeled by the PaSR model, [16], in which the filtered reaction rates are evaluated as the product of the reaction rates of the fine structures and their volume fraction. The LES equations are solved using a fully compressible semi-implicit finite volume discretization, based on the C++ library OpenFOAM, [17], with a monotonicity preserving flux reconstruction scheme and a Crank-Nicholson time integration. Most gas turbines operate on hydrocarbon fuels and here global three-step reaction mechanisms for CH_4-air, C_3H_8-air and $C_{12}H_{23}$-air combustion are used. These mechanisms are constructed from detailed reaction mechanisms using the methodology proposed by Meredith & Black, [18].

3. Validation and Supersonic Combustion Characteristics

The computational methodology used, involving the OpenFOAM library, [17], has been verified for a range of cases using systematic grid refinement studies, the method of manufactured solutions (MMS) and modified equations analysis

(MEA) to estimate the truncation errors. The application codes are extensively validated against DNS or experimental data, and many such cases have been reported earlier, most performed with LES, but also some with RANS to provide a reference to current engineering capabilities. Some of the flows considered includes the Taylor Green flow, [19], homogeneous isotropic turbulence, [20], fully developed turbulent channel flow, [21], flow past different blunt or streamlined bodies, [22-23], supersonic flows, [24-25], and reacting flow in different laboratory combustors. Figure 1 shows some representative results from the low-swirl burner of Cheng *et al.*, [26], studied experimentally by Peterson *et al.*, [27], and computationally by Nogenmyr *et al.*, [28], and the Triple Annual Research Swirler (TARS) studied experimentally by Li & Gutmark, [29], and computationally by Fureby *et al.*, [30]. These and other similar verification and validation studies give us confidence in the computational models and methods as well as the procedures used to investigate and evaluate the numerical results.

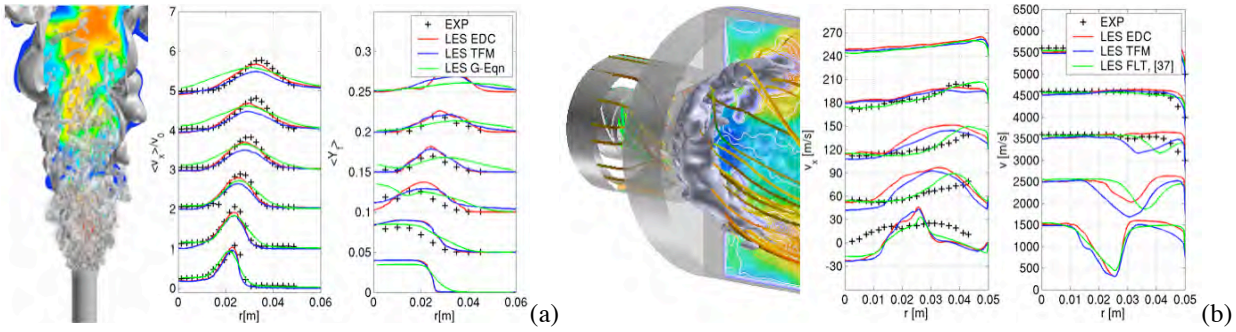

Figure 1. Validation and verification. (a) Perspective view of the low swirl burner together with comparisons of predicted and measured axial velocity and fuel mass fraction and (b) perspective view of the flow through the TARS and comparisons of predicted and measured axial velocity.

4. Aeropropulsion Gas Turbine Combustor Model

The aeropropulsion gas turbine combustor of interest in this study is of the reverse-flow type and is shown in figure 2a, and is mainly used for turboprop engines, [11]. The combustor casing accommodates two igniters for engine start and twelve fuel-air spray nozzles. Air enters through a diffuser and is lead through the air channel into the fuel-air spray nozzles, figure 2b, where the air is mixed with fuel prior to being discharged into the flame tube. The remaining air fills the space between the flame tube and the combustor wall, providing cooling of the flame tube walls and dilution of the primary combustion zone through a large number of film cooling and dilution holes. The flame tube consists of curved elements with built-in film cooling holes attached to the combustor casing using brackets. Two computational models, of which the first consists of a single 30° sector with periodic boundary conditions, and the second of the fully annular combustor, have been generated with about 3 and 36 million cells, respectively, cf. figure 2c. In order to be able to resolve all details of the fuel-air spray nozzles and film cooling holes, unstructured tetrahedral grids with local refinement patches in critical regions have been employed throughout. Conventional open inflow/outflow boundary conditions for all dependent variables have been utilized together with isothermal no-slip wall boundary conditions. The initial conditions for the combustion LES were obtained from an initial single sector RANS computation that in the case of the fully annular configuration was mapped onto the full annular domain. The nominal Reynolds number, based on the mass flow through the fuel-air spray nozzle, is $Re \approx 2 \cdot 10^6$ whereas the nominal combustor swirl number is $S \approx 0.5$.

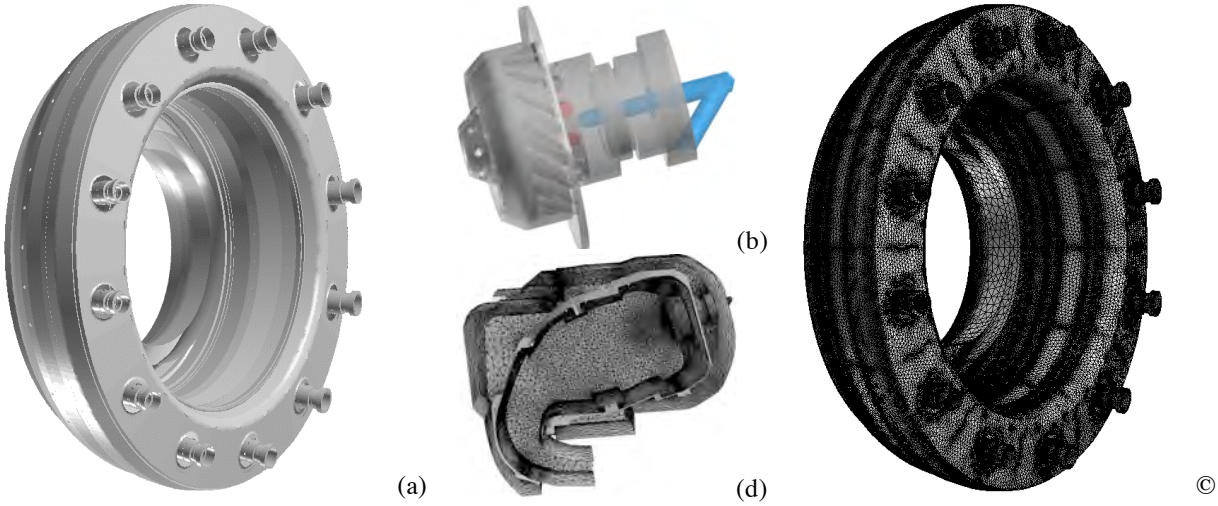

Figure 2. (a) Perspective view of the aeropropulsion gas turbine combustor with the twelve fuel-air spray nozzles, (b) detailed view of a fuel-air spray nozzle, (c) annular combustor grid and (d) detailed view of the combustor cross-sectional profile with the unstructured grid following the geometry.

5. Results, Comparison and Discussion

Figure 3a shows a perspective view of the interacting flames in the annular multi-burner configuration in terms of semi-transparent iso-surfaces of the temperature, whereas in figures 3b and 3c similar images are shown for sector 12 of the annular multi-burner configuration and for the single-sector configuration, respectively. At the first glance, the temperature distributions of the annular multi-burner configuration, shown in figures 3a and 3b, is similar to that of the single sector configuration in figure 3c, with the high temperature region lifted away from the fuel-air spray nozzles as seen in figures 3d and 3e. However, when studying the individual flames of the annular multi-burner configuration in figure 3a it is evident that these twelve flames are individually different, and that they are interacting with each other. The single sector configuration may be a reasonable representative of the annular multi-burner configuration in terms of mean quantities, but will not be able to represent any of the dynamics caused by the interacting flames and/or by features caused by azimuthal pressure waves. Under conditions when flame-to-flame interactions are strong, e.g. when combustion instabilities occur, the mean quantities may differ significantly between the single sector and multi-burner configurations. In single sector configurations (as well as in can combustors) longitudinal pressure fluctuations typically prevail, [31], whereas azimuthal pressure fluctuations are most likely to develop in annular configurations, [32], and thus provide the mechanisms for how neighboring flames interact with each other, [9-10].

The dynamics of the flames are dominated by the local equivalence ratio, i.e. the local fuel and oxygen distributions, the local pressure and the velocity gradients in the shear layers surrounding the flames (potentially responsible for quenching). The local equivalence ratio is governed by the fuel air mixture around the flame, i.e. the amount of air entrained in the fuel discharged through the nozzle, which in turn is affected by the local flow field and the turbulence in the vicinity of the fuel-air spray nozzle. These issues are reasonably well understood, being local in nature, whereas the influence of the unsteady pressure fluctuations is more complicated, having the ability to connect different parts of the combustor with each other. The velocity distributions in figures 3d and 3e show conically expanding high-speed zones developing around each fuel-air spray nozzle and high-speed jets discharging into the combustor through the film and dilution holes. In addition, a multiply-connected central recirculation region, with complex topology, is formed downstream of the air-fuel spray nozzles whereas semi-connected toroidal shaped recirculation zones are formed between the rear wall of the inner flame tube, the

fuel-air spray nozzles and the flames that stabilize around the central recirculation region. The hot combustion products are diluted by the air flowing through the dilution and mixing holes in the inner flame tube wall. As seen in figures 3d and 3e these air jets also cool the exhaust cases, reducing also the formation of post flame NO downstream of the flame zone. Further downstream in the flame tube the velocity increase due to the volumetric expansion, producing the desired high-speed flow to the turbine.

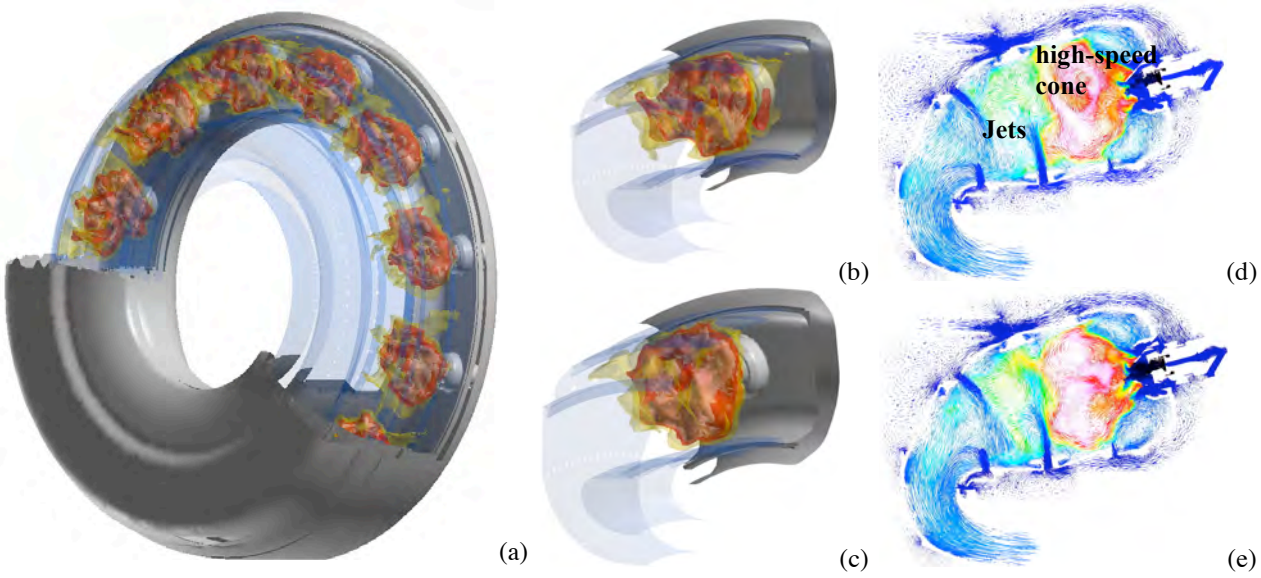

Figure 3. Instantaneous semi-transparent iso-surfaces of the temperature at 2500 K, 2000 K, 1500 K and 1000 K for the (a) annular multi-burner configuration (b) enlargement of burner 12, (c) single sector combustor, and velocity distributions colored by temperature on the centerplane from (d) the single sector configuration and (e) the annular multi-burner configuration.

The pressure fluctuation field, p', is a global quantity, the behavior of which is governed by the inhomogeneous wave equation, $\partial_t^2(p')-c^2\nabla^2(p')\approx(\gamma-1)\partial_t\dot{Q}-p_0\gamma\|\nabla\tilde{v}\|^2$, in which c is the speed of sound. The right-hand-side terms are source terms generating pressure fluctuations due to the unsteady heat-release, $\dot{Q}$, and the turbulent velocity fluctuations, respectively. For the cold fuel and air, $c\approx380$ m/s, whereas for the hot combustion products $c\approx900$ m/s, making pressure waves traversing different parts of the combustor at different time scales. In figure 4 we present side and rear views, respectively, of the predicted instantaneous pressure fluctuation field on the inner flame tube wall of the annular multi-burner configuration. As observed, the instantaneous pressure fluctuations form a very complicated pattern that is dominated by a combination of longitudinal, radial and azimuthal waves. In order to investigate this combination of pressure modes in greater detail a spectral analysis of the pressure fluctuations along four circumferential curves, shown in figure 4b, is carried out, and presented in figure 4c. Three of the circumferential curves in figure 4c are within the flame tube, at different distances from the fuel nozzle, whereas the fourth is from a location between the flame tube and the combustor casing. Based on geometrical considerations, the acoustic frequency of azimuthal pressure fluctuations should be around $f_{az}\approx c/(2\pi R_0)\approx950$ Hz, where R_0 is the mean radius of the annular combustor, whereas longitudinal pressure fluctuations typically occur at frequencies on the order of $f_{long}\approx c/L\approx1600$ Hz, where L is the length of a streamline traversing the combustor. From figure 4c we find that the spectral content varies between locations investigated, and that between the combustor casing and flame tube the spectral contents is determined by the distance between the fuel-air spray nozzles, and within the flame tube the spectral content is determined by a blend of azimuthal, radial and longitudinal pressure fluctuations. Close to the fuel-air spray

nozzles longitudinal modes dominate, whereas further downstream in the combustor both longitudinal and azimuthal modes coexist.

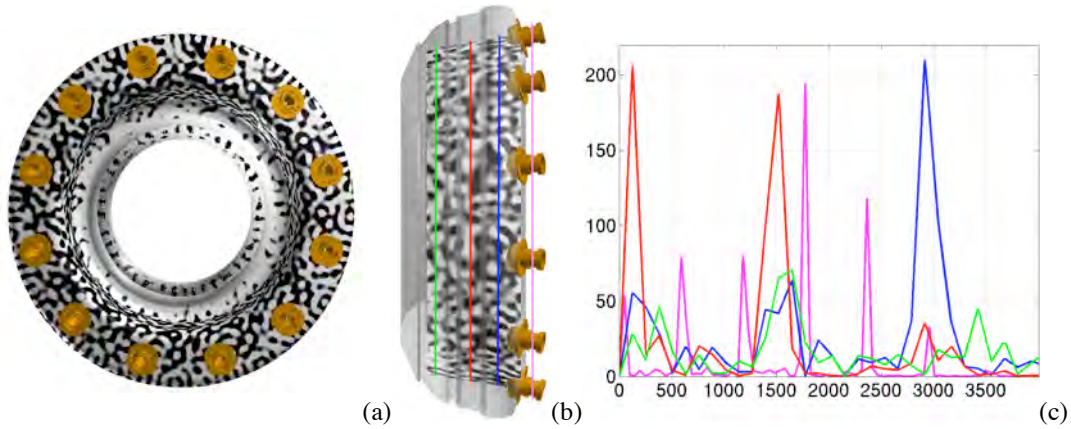

Figure 4. Contours of the pressure fluctuations on the inner flame tube wall on the annular multi-burner configuration as seen from the rear (a) and side (b), whereas (c) shows the spectral composition of the pressure field close to the fuel nozzle (—), at mid combustor (—), at rear combustor (—) and between flame tube and combustor casing (—).

Figure 5 shows instantaneous contours of the velocity magnitude, temperature, $C_{12}H_{23}$, CO, CO_2 and NO mass fractions, respectively, on a conically shaped plane parallel to centerlines of the fuel-air spray nozzles. This comparison is intended for deepening the understanding of the flow, injection, mixing and combustion process in the annular multi-burner configuration and to illustrate the effects of the azimuthal pressure fluctuations. Figure 5a shows that the central recirculation zones are individually different, being embedded in conically-shaped patches of high-speed air surrounding the centrally discharging fuel jets. Downstream, the airflow discharging through the dilution holes partially blocks the flow through the flame tube thereby giving raise to wakes and associated vortex structures enhancing mixing between the hot combustion products and the dilution air. The temperature in figure 5b reveals that the flames are located within the conically-shaped patches of high-speed air, with the high temperature regions detached from the fuel-air spray nozzles and located close to the most downstream parts of the central recirculation region. Furthermore, the air discharging through the dilution holes results in breaking-up the high temperature regions and cooling the exhaust gases that subsequently enters the turbine. Higher temperatures are also observed in the toroidal vortex structures surrounding the flames due mainly to the interactions between neighboring vortex structures. As mentioned, the flames in the annular multi-burner configuration are different from those obtained in the single-sector configuration. The reason for this is the global effects of the pressure fluctuations in figure 4. Moreover, the flames are observed to oscillate azimuthally, moving from top to bottom at a frequency close to 950 Hz. This azimuthal motion is accompanied by a weak longitudinal displacement of the flames and the central recirculation region. CO (figure 5d) is produced in the first segment of the flame-tube by the reaction $C_{12}H_{23}+11.75O_2 \rightarrow 12CO+11.5H_2O$ in regions where $C_{12}H_{23}$ (see figure 5c) and O_2 exist simultaneously as in the stratified regions of the fuel funnel where the mixing is sufficiently intense to mix $C_{12}H_{23}$ and O_2, and the temperature is high enough to initiate the reaction. This occurs in regions of high turbulence in the annular air jet surrounding the fuel nozzle. CO formed in the fuel-air reaction step is further oxidized to CO_2 (figure 5e) according to $CO+0.5O_2 \rightarrow CO_2$ near the end of the first stage of the flame tube where additional air is supplied through the dilution holes. These dilution air jets do not only increase the local mixing rates but also the reaction rates of this second reaction step by increasing the local turbulence levels. Moreover, the cooling provided by

the dilution jets aids to reduce the CO_2 emission levels. NO (figure 5f) is formed further downstream in the combustor by the much slower and temperature sensitive global reaction $N_2+O_2 \rightarrow 2NO$. In this particular investigation, the global NO reaction rate is selected to account for both thermal NO and prompt NO as suggested and outlined in [33].

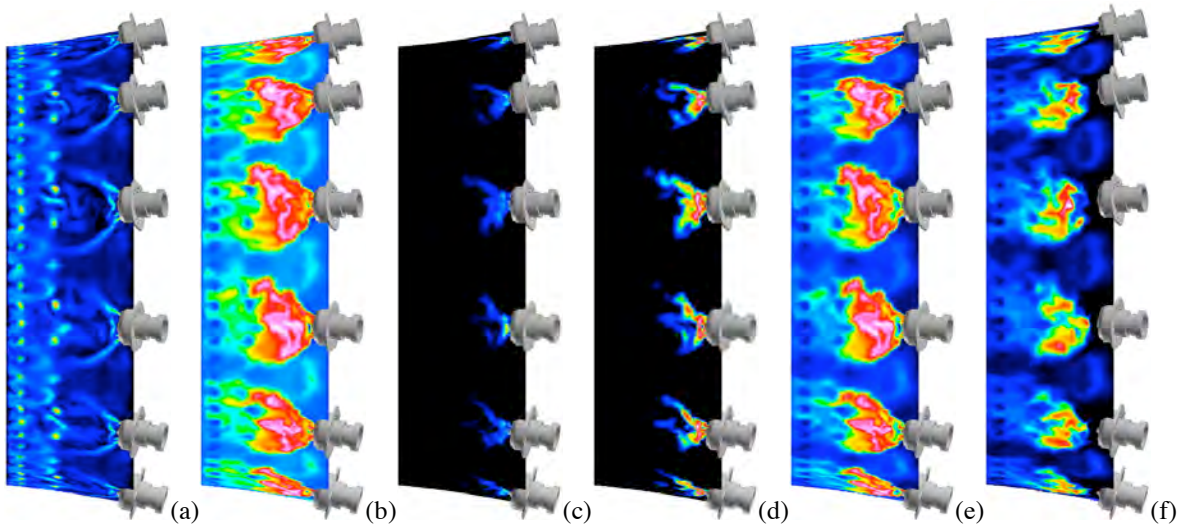

Figure 5. Contours of the (a) velocity magnitude, (b) temperature, (c) fuel mass fraction, (d) CO mass fraction, (e) CO_2 mass fraction and (f) NO mass fraction on a conically shaped plane parallel to centerlines of the fuel-air spray nozzles in the annular multi-burner configuration.

An important objective of this study is to improve our understanding of the unsteady combustion dynamics, in particular for the annular multi-burner configuration. As discussed earlier, the pressure fluctuation field, p', is related to the unsteady heat release, $\dot{Q}$, through the unsteady wave equation, $\partial_t^2(p')-c^2\nabla^2(p') \approx (\gamma-1)\partial_t\dot{Q}-p_0\gamma\|\nabla\tilde{\mathbf{v}}\|^2$, with the source terms representing unsteady heat-release and turbulent velocity fluctuations, respectively. By combining this unsteady wave equation with the linearized momentum equation, $\rho_0\partial_t(\mathbf{v}') \approx -\nabla p'$, an equation for the total acoustic energy, $\mathcal{E}=\frac{1}{2}(p'^2/\rho_0c^2+\rho_0|\mathbf{v}'|^2)$, is obtained that takes the general form $\partial_t(\mathcal{E})+\nabla\cdot\mathcal{F} \approx (\gamma-1)(p'\dot{Q})/(\rho_0c^2)$, in which $\mathcal{F}=p'\mathbf{v}'$ is the acoustic energy flux, whereas the source term is the correlation between the pressure fluctuations and the unsteady heat release. If the pressure fluctuation field and the unsteady heat release are in phase the amplitude of the acoustic energy will increase, whereas if the pressure fluctuation field and the unsteady heat release are out of phase the acoustic energy will decrease. This is the mathematical version of Lord Rayleigh's statement, [34], which can be used to examine the sensitivity to combustion instabilities which will occur if p' and $\dot{Q}$ are in phase. In figure 6a and 6b we show contours of Takeno's flame index, $FI=\nabla\tilde{Y}_{C_{12}H_{23}}\nabla\tilde{Y}_{O_2}$, and the heat- release, $\dot{Q}$, on a conically shaped plane parallel to centerlines of the fuel-air spray nozzles. From the distribution of FI we find that the flame is primarily a non-premixed flame (with $FI<0$ as the gradients of fuel and oxidizer oppose one another) but with a premixed core (with $FI>0$ as the gradients of fuel and oxidizer are parallel to each other) situated just outside of the fuel-air spray nozzles. This premixed core help stabilizing the flame. The heat-release field, $\dot{Q}$, show a similar topology as FI, essentially made up of a bi-modal structure with each of these layered structures resulting from the $C_{12}H_{23}$-air reaction $C_{12}H_{23}+11.75O_2 \rightarrow 12CO+11.5H_2O$ as well as the CO-air reaction $CO+0.5O_2 \rightarrow CO_2$, respectively. The flame tips are clearly interacting with each other and the flames clearly behave independently of each other due to the local flow field and the small but important variations in fuel supply to the individual fuel-air spray nozzles. In figure 6c we com-

pare the temporal evolution of the volumetrically integrated unsteady pressure fluctuations, $p'_v=\frac{1}{V}\int_V(p')dV$, and the volumetrically integrated unsteady heat release, $\dot{Q}_v=\frac{1}{V}\int_V(\dot{Q})dV$ between the single sector and annular multi-burner configurations. The p'_v traces show similar amplitudes for both cases whereas the $\dot{Q}_v$ trace for the annular multi-burner configuration shows higher amplitudes than for the single sector case. The mean heat release for the multi-burner case is somewhat lower than for the single sector case whereas the mean pressure is similar for both configurations. The dynamics of p'_v and $\dot{Q}_v$ are also different between the configurations, which also is manifested in the flame tube pressure variations discussed previously.

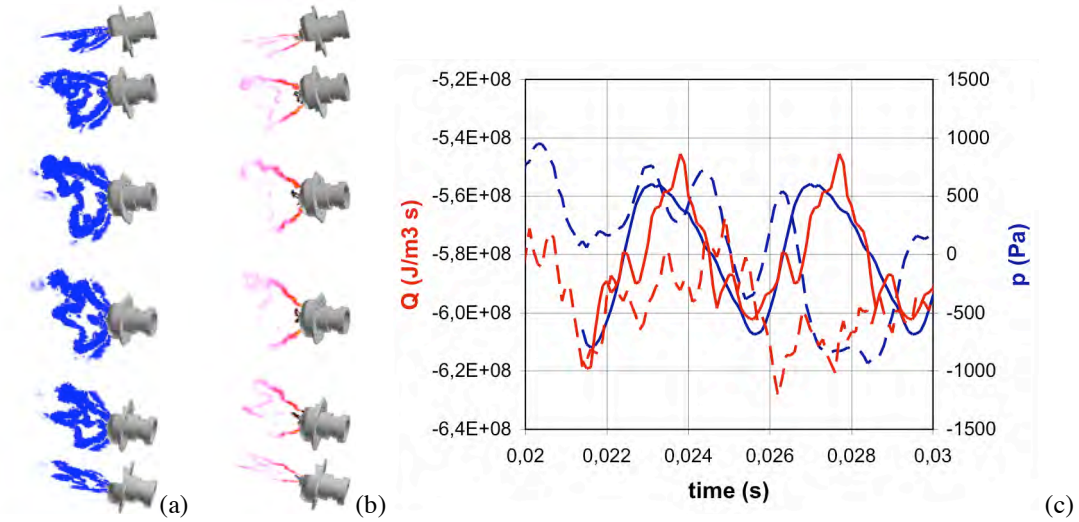

Figure 6. Contours of (a) Takeno's flame index and (b) the unsteady heat release, and (c) time series of volumetrically integrated pressure fluctuations (blue) and heat release (red) from the single sector (dashed) and annular multi-burner (solid) configurations.

6. Summary and Concluding Remarks

In this investigation we examine flow, mixing and combustion in an aeropropulsion gas turbine combustor. The analysis was performed by using a Large Eddy Simulation based Partially Stirrer Reactor (LES-PaSR) simulation model on a 30° single-sector combustor configuration with periodic side boundaries, emulating a multi-burner annular configuration, and a multi-burner annular configuration containing twelve 30° sectors. The single sector LES predictions and the multi-burner LES predictions share some basic features of the flow, mixing and combustion, but differ significantly in terms of the overall combustion dynamics. Based on the multi-burner annular LES predictions we conclude that a multiply-connected central recirculation zone is formed just downstream of the fuel-air spray nozzles, due to vortex breakdown downstream of each fuel-air spray nozzle. In addition, multiply-connected toroidal vortices develop between the rear inner flame tube wall, the flame and the fuel-air spray nozzles. Behind each fuel-air spray nozzle a swirling diffusion flame, stabilized by a swirling premixed flame core, anchors in the central recirculation region. These diffusion flames are slightly lifted away from the fuel-air spray nozzles and oscillate in the longitudinal direction. Downstream of the flame zone the hot combustion products are mixed with cooler air discharging through the film cooling and dilution holes, resulting in exhaust gases significantly cooler and more diluted that the adiabatic flame temperature. The volumetric expansion due to exothermicity results in a velocity increase that is most pronounced towards the reverse part of the combustor. The individual flames are clearly interacting with each other and are also feed with fuel-air mixtures of marginally different equivalence ratios resulting in individually different flame dynamics. These features cannot be predicted by a

single sector model and requires a multi-burner annular model. The flame interactions are most significantly manifested through the combustion dynamics and the variations of global pressure and heat release with time being different for the two configurations.

Acknowledgement

The study was part of the European Commission 6th framework program on Cost Effective Small AiRcraft (CESAR) with contract number AIP5-CT-2006-030888. The authors acknowledge the collaboration with S.A. Borzov, N.V. Gusev and T.V. Stepanova of Zaporozhye Machine-Building Design Bureau State Enterprise named after Academician A.G. Ivchenko in performing this study.

References

[1] Poinsot T. & Veynante D.; 2001, "Theoretical and Numerical Combustion", Edwards, Philadelphia, USA.

[2] Andreini A., Facchini B., Mangani L., Asfi A., Ceccherini G. & Modi R.; 2005, "NOx Emissions Reduction in an Innovative Industrial Gas Turbine Combustor (GE 10 Mashine): A Numerical Study of the Benefits of a New Pilot-system on Flame Structure and Emissions", Proc. ASME Turbo Expo, **2**, p 235.

[3] Janicka J. & Sadiki A.; 2005, "Large Eddy Simulation of Turbulent Combustion Systems, Proc. Comb. Inst. **30**, p 537.

[4] Pitsch H.; 2006, "Large Eddy Simulation of Turbulent Combustion", Annu. Rev Fluid Mech., **38**, p 453.

[5] Fureby C.; 2008, "LES Modeling of Combustion for Propulsion Applications", Phil. Trans. R. Soc. A, **367**, p 2957.

[6] Grinstein F.F., Margolin L. & Rider B. (Eds.); 2007, "Implicit Large Eddy Simulation: Computing Turbulent Fluid Dynamics", Cambridge University Press.

[7] Cannon S.M., Smith C.E. & Anand M.S.; 2003, "LES Predictions of Combustor Emissions in an Aero Gas Turbine Engine", AIAA 2003-4521.

[8] Grinstein F.F. & Fureby C.; 2004, "LES Studies of the Flow in a Swirl Gas Combustor", Proc. of the 30th Int Symp on Comb, p 1791.

[9] Staffelbach G., Gicquel L.Y.M. & Poinsot T.; 2007, "Highly Parallel Large Eddy Simulations of Multiburner Configurations in Industrial Gas Turbines", In Lecture Notes in Computational Science and Engineering, **56**, p 325.

[10] Fureby C.; 2010, "LES of a Multi Burner Annular gas Turbine Combustor", Flow Turb. & Comb., **84** p 543.

[11] Stepanov I.; 2006, "Selection of Thermodynamic Parameters, Construction and an Aircraft GTE Concept. revealing the Problems Connected to Development of Advanced Turboprop Engine for Light Aircraft", Contract No: AIP5-CT-2006-030888.

[12] Oran E.S. & Boris J.P.; 2001, "Numerical Simulation of Reactive Flow", Cambridge University Press, Cambridge, UK.

[13] Levine R.D.; 2005, "Molecular Reaction Dynamics", Cambridge university press.

[14] Menon S. & Fureby C.; 2010, "Computational Combustion", In Encyclopedia of Aerospace Engineering, Eds. Blockley R. & Shyy W., John Wiley & Sons.

[15] Bensow R. & Fureby C., 2006, "On the Justification and Extension of Mixed Models in LES", J Turbulence **8**, p N54.

[16] Baudoin E., Nogenmyr K.J., Bai X.S. & Fureby C.; 2009, "Comparison of LES Models applied to a Bluff Body Stabilized Flame", AIAA 2009-1178.

[17] Weller H.G., Tabor G., Jasak H. & Fureby C.; 1997, "A Tensorial Approach to CFD using Object Oriented Techniques", Comp. in Physics, **12**, p 629.

[18] Meredith K.V. & Black D.L.; 2006, "Automated Global Mechanism Generation for use in CFD Simulations", AIAA 2006-1168.

[19] Drikakis D., Fureby C., Grinstein F.F. & Youngs D.; 2007 "Simulations of Transition and Turbulence Decay in the Taylor-Green Vortex with the MILES Approach", J. Turbulence **8**, p 1.

[20] Fureby C., Tabor G., Weller H. & Gosman D.; 1997, "A Comparative Study of Sub Grid Scale Models in Isotropic Homogeneous Turbulence", Phys. Fluids, **9**, p 1416.

[21] Fureby C., Alin N., Wikström N., Menon S., Persson L., & Svanstedt N.; 2004, "On Large Eddy Simulations of High Re-number Wall Bounded Flows", AIAA.J. **42**, p 457.

[22] Fureby C., Tabor G., Weller H.G. & Gosman D.; 1999, "Large Eddy Simulation of the Flow Around a Square Prism", AIAA.J, **38**, p 442.

[23] Persson T. M. Liefevendahl, Bensow R. & Fureby C., 2006, "Numerical Investigation of the Flow over an Axisymmetric Hill using LES, DES and RANS", J. Turbulence, **7**, p 1.

[24] Fureby C., Knight D. & Kupiainen M.; 2007, "Compressible Turbulent Shear Flows", In Implicit Large Eddy Simulation: Computing Turbulent Fluid Dynamics, Eds. Grinstein F.F., Margolin L. & Rider B., Cambridge University Press, p 329.

[25] Fureby C., Henriksson M., Parmhed O., Sjökvist L. & Tegnér J.; 2008, "CFD Predictions of Jet Engine Exhaust Plumes", AIAA 2008-2345.

[26] Shepherd I.G., Cheng R.K., Plessing T., Kortschik C. & Peters N., 2002, "Premixed Flame Front Structure in Intense Turbulence", 29th Int. Symp. on Comb., p 1833.

[27] Petersson P., Nauert A., Olofsson J., Brackman C., Seyfried H., Zetterberg J., Richter M., Dreizler A., Geyer D., Linne A., Aldén M. & Cheng R.K.; 2007, "Simultaneous PIV/OH-PLIF, Rayleigh Thermometry/OH-PLIF and Stereo PIV Measurements in a low-swirl flame", Applied Optics, **46**, p 3928.

[28] Nogenmyr, K., Peterson P., Bai X.S., Aldén M. & Fureby C.; 2008, "A Comparative Study of LES Turbulent Combustion Models Applied to a Low Swirl Lean Premixed Burner", AIAA-2008 0513.

[29] Li G. & Gutmark E.; 2005, "Experimental Study on Boundary Conditions Effects on Non-reacting and Reacting Flow in a Multi-Swirl Gas Turbine Combustor", AIAA.J, **44**, p 444.

[30] Fureby C., Grinstein F.F., Li G. & Gutmark E.; 2006, "An Experimental and Computational Study of a Multi-Swirl Gas Turbine Combustor", 31st Int Symp on Comb., p 3107.

[31] Lörstad D., Lindholm A., Alin N., Fureby C., Lantz A., Collin R & Aldén M.; 2010, "Experimental and LES Investigation of an SGT-800 Burner in a Combustion Rig", Proceedings of ASME Turbo Expo 2010: Power for Land, Sea and Air, GT2010-22688.

[32] Pankiewitz C. & Sattlemayer T.; 2003, "Time Domain Simulation of Combustion Instabilities in Annular Combustors", J. Engng for Gas Turbines and Power, **125**, p 677.

[33] Zeldovich Y.B., Barenblatt G.I., Librovich V.B. & Makhviladze G.M.; 1985, "The. Mathematical Theory of Combustion and Explosions", Consultants Bureau, p 30, New York.

[34] Rayleigh J.W.S.; 1945, "The Theory of Sound", vol. II. New York: Dover.

Copyright Statement